Earth and Planetary Science Letters 325–326 (2012) 1–9

Contents lists available at SciVerse ScienceDirect

Earth and Planetary Science Letters

journal homepage: www.elsevier.com/locate/epsl

Rapid magma emplacement in the Karoo Large Igneous Province

Henrik Svensen [a,*], Fernando Corfu [b], Stéphane Polteau [a,c], Øyvind Hammer [a], Sverre Planke [a,c]

[a] Physics of Geological Processes, University of Oslo, PO Box 1048 Blindern, 0316 Oslo, Norway
[b] Department of Geosciences, University of Oslo, PO Box 1047 Blindern,0316, Oslo, Norway
[c] Volcanic Basin Petroleum Research, Forskningsparken, Gaustadalléen 21, 0349 Oslo, Norway

ARTICLE INFO

Article history:
Received 24 October 2011
Received in revised form 12 January 2012
Accepted 13 January 2012
Available online 21 February 2012

Editor: T.M. Harrison

Keywords:
Karoo
Large Igneous Province
global paleoclimate
U–Pb age
zircon
ID-TIMS

ABSTRACT

Understanding the dynamics of continental Large Igneous Provinces (LIPs) relies on precise dating of basaltic rocks. LIP research has traditionally focused on dating lavas, often neglecting the volumetrically important sill intrusions in underlying sedimentary basins. Here we present U–Pb zircon (and baddeleyite) ages for fourteen new samples of Karoo LIP sills and dykes spaced by as much as 1100 km across the half million square kilometer Karoo Basin. The samples yield remarkably coherent ages ranging from 183.0 ± 0.5 to 182.3 ± 0.6 myr. Probability modeling indicates that basin scale emplacement took place within an interval of about 0.47 myrs (less than 0.90 myrs with 95% confidence), and could even have represented a single magma emplacement event. Combining the new ages with the estimated volume of sills in the Karoo Basin gives an emplacement rate of 0.78 km^3/yr, which is higher than previous estimates. Upper crustal magma storage may account for these high rates. The results challenge the view that melt emplacement in a sedimentary basin is a prolonged process, support a scenario of pulsating catastrophic events within a narrow time frame, and strengthens the hypothesis linking LIPs and sill emplacement to global environmental crises.
© 2012 Elsevier B.V. All rights reserved.

1. Introduction

Continental LIPs are composed of surface lava flows and subsurface sill. In provinces like the $>3\times10^6$ km^2 Karoo LIP in South Africa and the $>2\times10^6$ km^2 Siberian Traps the volume of the sills is considerable, several times higher than that of the present-day exposed lava. Previous dating studies on the Karoo LIP have focused principally on the lavas and less on the sills, and with few exceptions (Encarnacion et al., 1996; Svensen et al., 2007) the available ages are mostly obtained using the $^{40}Ar/^{39}Ar$ method with uncertainties at best in the ±1.5 myr. range (Duncan et al., 1997; Jourdan et al., 2005; Jourdan et al., 2007). Based on an $^{40}Ar/^{39}Ar$ study of 15 sills in the eastern Karoo Jourdan et al. (2008) concluded that the Karoo sills were emplaced over a sustained magmatic period of some 3 myr., contrary to previous speculations about a single stage of sill emplacement (Svensen et al., 2007). However, the Ar system can be affected by subtle biases from Ar overpressure, retrogression or recoil phenomena which can be difficult to discriminate (Duncan et al., 1997; Jourdan et al., 2007), and prolonged cooling in thick sills may also have contributed to a spread of ages. As a consequence, understanding the details of the timing and duration of sill emplacement in the Karoo Basin has relied on qualitative arguments about field relations and is compromised by the paucity of available geochronological data.

We have now investigated these discrepant interpretations using the U–Pb method on zircons collected from sill intrusions across the Karoo Basin (Fig. 1). This technique has proven to be precise and reliable, especially due to the internal control offered by its twin ^{238}U and ^{235}U decay systems, which permit an internal verification of closed system behavior. Although zircons are normally absent in mafic rocks, they can be locally abundant in coarse grained and pegmatitic parts of sills and dykes. The Karoo Basin, the best exposed continental LIP with many accessible sills in outcrops, quarries and boreholes represents a natural laboratory with a unique possibility to unravel the age distribution of shallow intrusions on a LIP scale. The results have implications for constraining magma generation and LIP plumbing processes and to understand how Karoo magmatism relates to the global Toarcian oceanic anoxia and carbon cycle perturbation.

2. Magma emplacement in the Karoo Basin

Sills occur throughout the Karoo Basin, and up to 130 m thick sills are present in the basal glacial Dwyka Group. The thickest sills are up to 200 m thick and represent predominantly extensive (>200 km) sheets emplaced in the organic-rich shales of the Permian Ecca Group. Higher in the Karoo stratigraphy, sills are emplaced in the sandstone-dominated, fluvially deposited Beaufort Group and form nested saucer-shaped intrusions with individual thicknesses of

* Corresponding author. Tel.: +47 93053870; fax: +47 22 85 51 01.
E-mail addresses: hensven@fys.uio.no (H. Svensen), fernando.corfu@geo.uio.no (F. Corfu), stephane@vbpr.no (S. Polteau), oyvind.hammer@nhm.uio.no (Ø. Hammer), planke@vbpr.no (S. Planke).

0012-821X/$ – see front matter © 2012 Elsevier B.V. All rights reserved.
doi:10.1016/j.epsl.2012.01.015

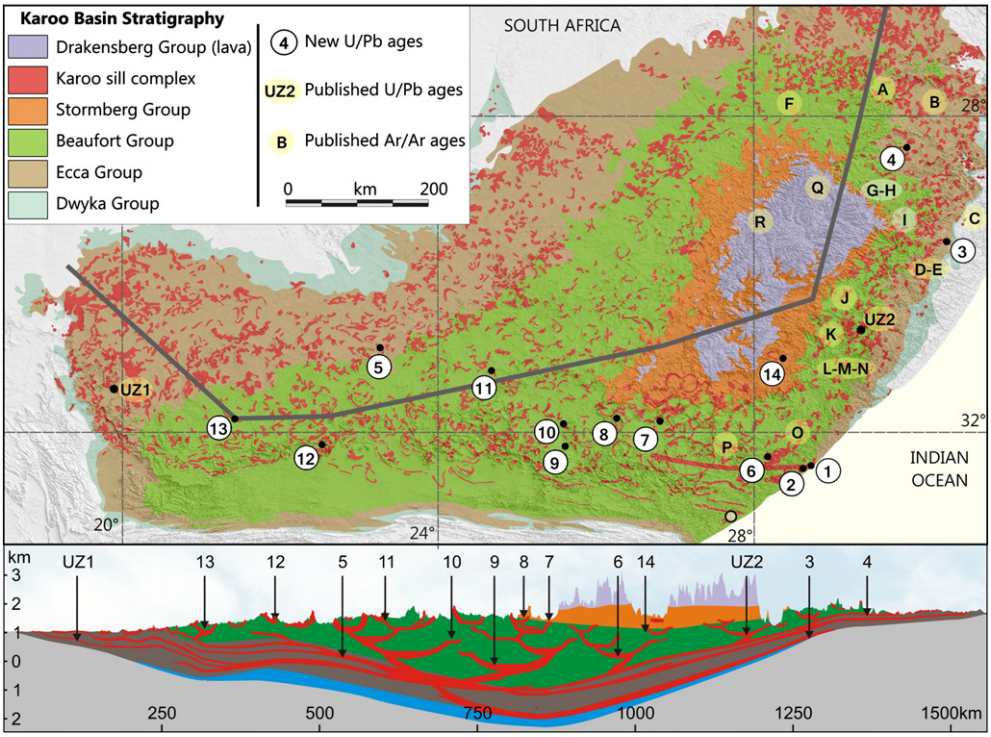

Fig. 1. Geological map of the Karoo Basin showing sampling sites. The gray line represents the regional cross section, where individual sampling sites are projected to their stratigraphic position. UZ1: U–Pb sample in Svensen et al. (2007), UZ2: U–Pb sample in Encarnacion et al. (1996), 1–14: U–Pb samples in this study (Table 1 and Supplementary Information), A–R: location of Ar–Ar dates quoted in the text.

~100 m and characteristic diameters of 20–60 km. Sills are less common in the uppermost part of the basin, the Stormberg Group (Catuneanu et al., 2005; Johnson et al., 1996; Smith, 1990) (Fig. 1) whereas dykes are common and form 120–180 km long lineaments such as the 100–200 m wide Gap Dykes. Sills are absent in the Drakensberg Group lavas, suggesting that they were emplaced prior to the main phase of flood volcanism or that emplacement within the lavas was prevented. The Karoo sills are dominantly tholeiitic basalts to basaltic andesites, although more evolved sills are also present locally (Marsh and Eales, 1984; Neumann et al., 2011). Most of the Karoo Basin sills are geochemically broadly similar to the Lesotho type basaltic lavas, the dominant lava type in the middle to upper part of the lava stratigraphy. Detailed geochemical investigations have shown that sills within the same region may have formed from separate batches of melt (Galerne et al., 2008).

Today, the sills comprise up to 30% of the Karoo Basin's thickness and are present within a 0.55×10^6 km^2 basin area representing at least 340,000 km^3 of dolerite (see Results) (Chevallier and Woodford, 1999; du Toit, 1920). Sill emplacement led to widespread phreatic and phreatomagmatic activity (McClintock et al., 2008; Svensen et al., 2006), and the release of thousands of gigatons of carbon gas from the contact metamorphosed organic-rich sediments around the sills (Svensen et al., 2007). The proposed link to the Toarcian global carbon cycle perturbation (Svensen et al., 2007) was recently strengthened by U–Pb bentonite dating and carbon chemostratigraphy in the Neuquén Basin, Argentina, suggesting an initiation of the Toarcian event at 182.16 ± 0.6 myr (Mazzini et al., 2010) thus overlapping the age of a sill intrusion in the western Karoo Basin and the early stage of flood basalt volcanism (Jourdan et al., 2005; Svensen et al., 2007).

The peak of volcanic activity in South Africa and Lesotho is recorded at 183 ± 1 myr by ^{40}Ar/^{39}Ar dating of the Drakensberg basalts and some Karoo Basin dykes and sills (Duncan et al., 1997; Jourdan et al., 2005; Jourdan et al., 2007). The volcanism may have been focussed in time as a small number of intense eruption periods (Moulin et al., 2011). It has also been proposed that two sill emplacement pulses separated by several million years are recorded in the eastern parts of the basin (Jourdan et al., 2008). The only sills dated using the U–Pb method on zircons gave ages of 182.5 ± 0.4 myr and 183.7 ± 0.6 myr (Encarnacion et al., 1996; Svensen et al., 2007). The latter is an anomalously thick intrusion in the south-eastern parts of the basin.

3. Methods

3.1. Sampling and petrography

We sampled coarse-grained to pegmatitic sills with high potential for extracting datable magmatic zircons and baddelyite. Samples were collected from boreholes, quarries, coastal exposures, river beds and road cuts. Cores were sampled at the core shed of the Council for Geoscience, Pretoria. Coarse and pegmatoidal sills were targeted specifically during a second stage of field work in 2008 after sampling of fine grained units in a 2007 campaign failed to yield datable zircons.

Pegmatites commonly occur both in patches (with diffuse boundaries up to 20–30 cm in diameter) and as 2–70 cm thick veins with sharp contacts to the surrounding dolerite. In addition to pegmatites, two types of gabbroic sills were sampled: a first type (K08-09) is from a gabbroic sill intruded in the upper part of the Karoo Supergroup stratigraphy and may represent an equivalent to the shallow-seated and strongly differentiated Bird River Complex (Eales and Robey, 1976); the second type (sample K08-41) is a leucocratic and granophyric dolerite (diorite to granodiorite, rich in intergrowths of quartz and K-feldspar) that has a typical lighter color due to the more felsic composition. Additionally, at the Spilmanskop locality in the Cradock district (sample K08-48), a granodiorite sheet is associated with disseminated sulfides. Finally, the Gap Dyke (SP-07-05 and SP-06-05)

consists of coarse-grained leucocratic and granophyric dolerite, and contained local fine-grained dolerite xenoliths up to 10 m in diameter.

The degree of alteration of the primary igneous dolerite minerals varies from fresh to intense sericitization of plagioclase and alkali feldspar, chloritization of amphibole and pyroxenes, and calcite in the most altered sample (K08-01). Sample K08-47 is distinguished from the rest by the presence of epidote and pervasive chloritization of amphibole and pyroxene. A more detailed description of the individual samples, locations and coordinates is given as Supplementary Data.

3.2. U–Pb analytical procedure

The samples were crushed and milled, followed by a preconcentration of the heavy mineral fraction using a Wilfley table, before extracting zircon and baddeleyite using a Frantz magnetic separator and methylene iodide flotation. Isotopic analyses of U–Pb in zircon and baddeleyite were carried out by ID-TIMS following a modified procedure of Krogh (1973); details of the routines in the Oslo laboratory are given in Corfu (2004). The best zircon grains were handpicked and abraded, either mechanically (Krogh, 1982) or chemically (Mattinson, 2005), in order to remove altered and disturbed domains. The ages are calculated using the decay constants of Jaffey et al. (1971), and the data are regressed using the program Isoplot (Ludwig, 2003).

3.3. Monte Carlo simulations

To further constrain the sill emplacement duration we have done probability modeling. The assumption made is that the ages represent a prolonged emplacement phase, and that the spread is due to both real age differences and dating uncertainties. To put bounds on the duration of the magmatic phase, we assumed that the emplacement proceeded with Gaussian intensity through time, and that the observed normal distribution of the U–Pb ages (Shapiro–Wilk $W = 0.94$, $p = 0.39$) reflects this intensity distribution. We generated 50,000 simulations of 15 emplacement events distributed randomly in time with a given standard deviation (duration) of σ_{sim}, each event with an added simulated dating error drawn from the given set of errors. For a given σ_{sim}, this allows the estimation of a one-tailed probability of the standard deviation of the dates as large as observed. The σ_{sim} was then allowed to vary (in an outer loop) through a range of durations, giving a complete cumulative probability function as a function of duration.

The idea behind this procedure is to simulate the sequence of processes leading to the final set of radiometric dates, over a range of possible durations for the emplacement phase. To summarize, we first assign random true ages to the 15 emplacement events, using the assumed intensity curve through time. Then we simulate the radiometric dating by adding to these true dates random errors with deviations drawn from the actual set of estimated radiometric errors. Repetition of this randomized procedure gives a histogram (probability distribution) of resulting standard deviations of the set of radiometric dates, which can be compared with the observed spread in radiometric dates. The whole procedure is repeated over a range of emplacement durations. The C code can be obtained from the authors.

4. Results

4.1. Karoo Basin cross section and sill volume

The regional profile presented in this contribution (Fig. 1) is constrained by borehole and surface geology data. We used a series of 21 deep stratigraphic boreholes that intersect portions of the Beaufort Group, the organic-rich Ecca Group, and terminate in the Dwyka glaciogenic sediments or Precambrian basement lithologies. Original well completion and log reports are available at the Council for Geoscience in Pretoria. The presented geological map is simplified from the 1:1,000,000 lithostratigraphic map from the Council of Geoscience downloaded at onegeology.org.

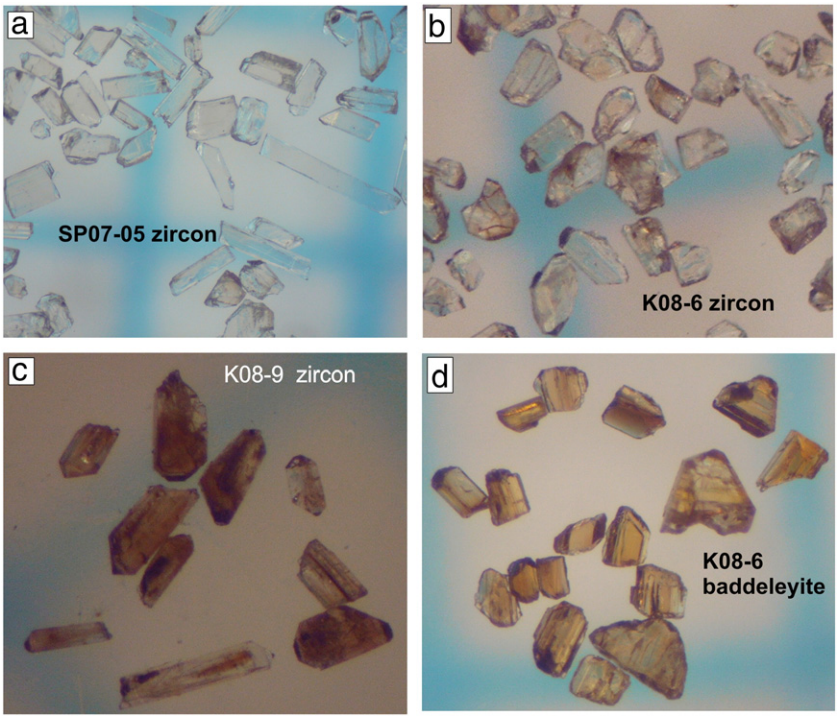

Fig. 2. Typical appearance of zircon in samples from this study. Zircon crystals are commonly long-prismatic, but often fragmented. They range from high quality, clear and non-metamict crystals, such as in SP07-05 (a), to crystals of intermediate quality such as in K08-06 (b), to variably metamict and locally altered prisms such as in K08-9 (c). (d) Baddeleyite in sample K08-6; this mineral is present in several of the samples, but mostly as blades that are too thin to abrade and hence will likely give too young ages due to Pb loss from its margins.

Table 1
U–Pb data for zircon and baddeleyite for Karoo LIP.

Mineral characteristics[a]	Weight[b]	U[b]	Th/U[c]	Pbc[d]	$^{206}Pb/^{204}Pb$[e]	$^{207}Pb/^{235}U$[f]	±2σ	$^{206}Pb/^{238}U$[f]	±2σ	rho	$^{207}Pb/^{206}Pb$[f]	±2σ	$^{206}Pb/^{238}U$[f]	±2σ	$^{207}Pb/^{235}U$[f]	±2σ	$^{207}Pb/^{206}Pb$[f]	±2σ
	(μg)	(ppm)		(pg)			(abs)		(abs)			(abs)	(myr)					
QU 1-2, pegmatite in dolerite sill; (lat: −31.83; long: 21.44; #13 in Fig. 1)																		
Z eu fr cl [9]	4	3432	2.52	2.2	11,269	0.19746	0.00048	0.02875	0.00006	0.91	0.04982	0.00005	182.7	0.4	183.0	0.4	186.6	2.3
Z eu fr b [4]	5	3791	2.40	2.7	12,465	0.19719	0.00048	0.02874	0.00006	0.92	0.04976	0.00005	182.7	0.4	182.7	0.4	183.8	2.2
K08-31, pegmatite in dolerite sill, Beaufort West road; (lat: −32.25; long: 22.56; #12)																		
Z eu fr cl [1]	1	374	1.22	0.9	800	0.19858	0.00206	0.02883	0.00010	0.44	0.04996	0.00047	183.2	0.6	183.9	1.7	193.1	21.7
Z eu fr cl [1]	1	755	1.31	0.7	1875	0.19769	0.00115	0.02868	0.00011	0.70	0.04999	0.00021	182.3	0.7	183.2	1.0	194.6	9.6
Z eu fr cl [1]	1	607	1.46	1.0	1093	0.19659	0.00166	0.02864	0.00013	0.55	0.04978	0.00035	182.0	0.8	182.2	1.4	184.7	16.4
K08-34, pegmatite in dolerite sill, Britstown; (lat: −30.91; long: 23.26; #3)																		
Z eu fr cl [1]	1	273	2.31	0.8	629	0.19953	0.00281	0.02892	0.00021	0.57	0.05004	0.00058	183.8	1.3	184.7	2.4	196.7	26.8
Z eu bp cl-b [1]	1	7136	3.42	0.9	14,599	0.19761	0.00064	0.02878	0.00009	0.92	0.04979	0.00006	182.9	0.6	183.1	0.5	185.3	3.0
Z eu fr cl [1]	1	561	2.11	0.8	1271	0.19756	0.00147	0.02866	0.00012	0.60	0.05000	0.00030	182.1	0.8	183.1	1.2	194.8	13.8
K08-41, coarse-grained leucodolerite sill; (lat: −31.21; long: 24.66; #11)																		
Z eu fr cl-b [1]	1	3157	2.17	1.3	4274	0.19708	0.00106	0.02881	0.00015	0.80	0.04961	0.00016	183.1	0.9	182.6	0.9	176.6	7.7
Z eu fr cl-b [1]	1	957	2.05	1.1	1614	0.19689	0.00122	0.02873	0.00010	0.62	0.04971	0.00024	182.6	0.6	182.5	1.0	181.4	11.3
Z eu fr cl-b [1]	1	1385	3.41	1.5	1648	0.19624	0.00147	0.02857	0.00018	0.69	0.04982	0.00027	181.6	1.1	181.9	1.2	186.4	12.7
K08-48, granodiorite; (lat: −31.90; long: 25.58; #10)																		
Z eu fr cl-b [3]	1	12,110	1.39	1.3	16,212	0.19783	0.00054	0.02879	0.00007	0.94	0.04984	0.00005	183.0	0.4	183.3	0.5	187.6	2.1
Z eu fr cl-b [7]	1	7689	1.23	0.8	16,893	0.19754	0.00050	0.02875	0.00006	0.94	0.04983	0.00004	182.7	0.4	183.0	0.4	187.3	2.1
Z eu fr b-w [1]	1	16,708	1.71	2.4	12,692	0.19732	0.00070	0.02872	0.00009	0.95	0.04984	0.00006	182.5	0.6	182.9	0.6	187.3	2.5
Z eu fr cl-b [3] *	1	22,181	1.34	3.2	12,290	0.19595	0.00061	0.02853	0.00008	0.96	0.04981	0.00004	181.4	0.5	181.7	0.5	186.1	2.1
K08-47, pegmatite in dolerite sill, Cradock; (lat: −32.16; long: 25.60; #9)																		
Z eu fr cl-b [9]	1	1382	1.27	1.1	2312	0.19730	0.00111	0.02879	0.00012	0.78	0.04970	0.00018	183.0	0.8	182.8	0.9	181.2	8.2
Z eu fr cl-b [6]	2	2200	1.39	0.7	12,110	0.19652	0.00062	0.02870	0.00009	0.91	0.04965	0.00007	182.4	0.5	182.2	0.5	178.8	3.0
Z eu fr cl-b [6] *	1	3786	1.59	1.8	3813	0.19606	0.00064	0.02859	0.00007	0.74	0.04973	0.00011	181.7	0.4	181.8	0.5	182.5	5.1
Z eu fr cl-b [16]	1	1912	1.87	4.7	750	0.19578	0.00231	0.02846	0.00029	0.85	0.04988	0.00031	180.9	1.8	181.5	2.0	189.6	14.4
SP06-05, granophyre, Gap Dyke, Qora Mouth; (lat: −32.44; long: 28.69; #1)																		
Z eu fr cl [42]	21	1274	1.38	1.7	29,084	0.19710	0.00053	0.02871	0.00007	0.94	0.04980	0.00005	182.5	0.4	182.7	0.4	185.5	2.1
Z eu fr cl [50]	12	1003	1.35	1.6	13,164	0.19715	0.00047	0.02871	0.00006	0.92	0.04981	0.00005	182.5	0.4	182.7	0.4	185.9	2.2
Z eu fr cl [17]	36	2394	1.37	2.2	69,342	0.19678	0.00056	0.02867	0.00007	0.97	0.04978	0.00004	182.2	0.5	182.4	0.5	184.9	1.7
SP07-05, granophyre, Gap Dyke, Qora Mouth; (lat: −32.44; long: 28.66; #2)																		
Z eu fr cl [20]	201	1069	1.16	4.9	78,852	0.19738	0.00058	0.02875	0.00008	0.98	0.04979	0.00003	182.7	0.5	182.9	0.5	185.4	1.4
Z eu fr cl [31]	87	1040	1.20	3.9	41,892	0.19711	0.00050	0.02872	0.00007	0.97	0.04978	0.00003	182.5	0.4	182.7	0.4	184.8	1.5
Z eu fr cl [10]	55	982	1.13	1.8	54,116	0.19698	0.00049	0.02870	0.00006	0.96	0.04978	0.00003	182.4	0.4	182.6	0.4	184.9	1.6

K08-1, pegmatite in dolerite sill, Butterworth Quarry; (lat: −32.33; long: 28.18; #6)																		
Z eu fr cl [12]	52	569	1.46	2.8	19,288	0.19810	0.00056	0.02883	0.00008	0.95	0.04984	0.00004	183.2	0.5	183.5	0.5	187.6	2.1
Z eu fr cl [21]	38	583	1.45	1.9	20,542	0.19759	0.00050	0.02875	0.00007	0.94	0.04985	0.00004	182.7	0.4	183.1	0.4	187.9	2.0
Z eu fr cl [30]	28	482	1.48	41.6	603	0.19761	0.00123	0.02876	0.00007	0.43	0.04984	0.00028	182.8	0.4	183.1	1.0	187.5	13.1
Z eu fr cl [2] *	7	586	1.25	1.5	5068	0.19636	0.00058	0.02868	0.00007	0.78	0.04965	0.00009	182.3	0.4	182.0	0.5	178.6	4.3
SP08-05, pegmatite in dolerite sill, offshoot of the Golden Valley; (lat: −31.84; long: 26.21; #8)																		
Z eu fr cl [17]	10	500	3.18	1.2	7295	0.19839	0.00055	0.02884	0.00007	0.80	0.04988	0.00008	183.3	0.5	183.8	0.5	189.6	3.9
Z eu fr cl [26]	14	1076	3.18	2.5	11,070	0.19787	0.00048	0.02879	0.00006	0.92	0.04985	0.00005	183.0	0.4	183.3	0.4	187.9	2.2
Z eu fr cl CA [25]	35	923	2.75	2.4	24,027	0.19780	0.00052	0.02879	0.00007	0.95	0.04982	0.00004	183.0	0.4	183.3	0.4	186.8	1.9
Z eu fr cl CA [23]	17	962	2.91	2.1	13,928	0.19770	0.00049	0.02878	0.00006	0.93	0.04983	0.00005	182.9	0.4	183.2	0.4	187.0	2.1
Z eu fr cl-b [12]	14	1021	3.59	2.2	11,899	0.19745	0.00048	0.02874	0.00006	0.93	0.04982	0.00005	182.7	0.4	183.0	0.4	186.6	2.1
Z eu fr cl [20]	15	356	2.95	1.5	6239	0.19721	0.00056	0.02871	0.00007	0.80	0.04982	0.00009	182.5	0.4	182.8	0.5	186.5	4.0
Z eu fr cl [20]	2	1500	3.56	0.8	6583	–	–	–	–	–	0.04981	0.00009	–	–	–	–	186.0	4.3
K08-6, pegmatite in dolerite sill, Hill Crest Quarry outside Queenstown; (lat: −31.89; long: 26.80; #7)																		
B eu fr b [8]	7	294	0.04	2.1	1817	0.19773	0.00100	0.02874	0.00009	0.53	0.04989	0.00022	182.7	0.6	183.2	0.8	190.0	10.0
Z eu fr cl-b [17]	33	1113	3.05	8.9	7411	0.19730	0.00048	0.02873	0.00006	0.94	0.04980	0.00004	182.6	0.4	182.8	0.4	185.8	1.9
Z eu fr cl [16]	25	1418	3.11	6.0	10,571	0.19683	0.00050	0.02868	0.00006	0.95	0.04978	0.00004	182.3	0.4	182.4	0.4	184.6	1.9
Z eu fr cl [22]	14	1924	3.65	7.3	6646	0.19660	0.00062	0.02866	0.00007	0.91	0.04975	0.00007	182.2	0.4	182.2	0.5	183.3	3.2
K08-9, gabbroic (granophyric) sill, McLear; (lat: −31.08; long: 28.35; #14)																		
Z eu fr cl [10]	7	1388	2.37	3.0	5851	0.19789	0.00053	0.02880	0.00007	0.86	0.04984	0.00007	183.0	0.4	183.3	0.5	187.4	3.1
B eu fr b [6]	1	649	0.14	1.4	837	0.19924	0.00252	0.02878	0.00024	0.61	0.05021	0.00051	182.9	1.5	184.5	2.1	204.9	23
Z eu fr b [1]	1	8727	2.07	1.4	11,608	0.19720	0.00054	0.02873	0.00007	0.93	0.04978	0.00005	182.6	0.4	182.8	0.5	184.6	2.3
Z eu fr b [1]	1	4000	2.20	0.5	14,563	0.19702	0.00051	0.02872	0.00007	0.89	0.04975	0.00006	182.6	0.4	182.6	0.4	183.1	2.7
Z eu fr cl-b CA [7]*	12	481	1.99	2.8	3781	0.19700	0.00056	0.02863	0.00006	0.79	0.04991	0.00009	181.9	0.4	182.6	0.5	190.8	4.2
K08-16, pegmatites in dolerite, Ladysmith–Newcastle; (lat: −28.37; long: 29.94; #5)																		
Z eu fr cl [1]	1	610	2.86	0.9	1306	0.19772	0.00143	0.02882	0.00012	0.62	0.04976	0.00028	183.1	0.7	183.2	1.2	184.0	13.2
Z eu fr cl-b [4]	1	1359	1.49	1.4	1745	0.19633	0.00133	0.02867	0.00014	0.73	0.04966	0.00023	182.2	0.9	182.0	1.1	179.3	10.7
Z eu fr cl-b [1]	1	262	1.62	0.6	821	0.19455	0.00289	0.02866	0.00032	0.70	0.04924	0.00053	182.1	2.0	180.5	2.4	159.2	24.8
Z eu fr cl t [1]	1	2199	1.80	0.8	4846	0.19619	0.00075	0.02865	0.00009	0.73	0.04966	0.00013	182.1	0.6	181.9	0.6	179.1	6.1
K08-13, pegmatite in dolerite, Pietermaritzburg Coedmore Quarry; (lat: −29.57; long: 30.43; #4)																		
Z eu fr cl [1]	1	10,815	2.21	1.7	11,773	0.19795	0.00053	0.02883	0.00007	0.92	0.04980	0.00005	183.2	0.4	183.4	0.4	185.8	2.4
Z eu fr b [1]	1	7278	1.76	0.9	14,734	0.19754	0.00054	0.02876	0.00007	0.91	0.04981	0.00006	182.8	0.5	183.0	0.5	186.2	2.6
Z eu fr cl-b [8]	1	9191	1.99	1.3	13,022	0.19702	0.00056	0.02870	0.00007	0.92	0.04979	0.00005	182.4	0.5	182.6	0.5	185.1	2.5
Z eu fr cl-b [1]	1	2040	1.47	0.5	7071	0.19720	0.00059	0.02869	0.00008	0.84	0.04986	0.00008	182.3	0.5	182.8	0.5	188.3	3.8
Z eu fr cl-b CA [10]	3	190	1.37	1.8	594	0.19490	0.00267	0.02853	0.00013	0.45	0.04954	0.00061	181.4	0.8	180.8	2.3	173.5	28.5

[a] Z = zircon; B = baddeleyite; eu = euhedral; fr = fragment; bp = bi-pyramid without prism; cl = clear; b = brown; w = white; t = some turbidity; [1] = number of grains; CA = treated with chemical abrasion calculation (all the others mechanically abraded); * not used in the age.

[b] Weight and concentrations are known to better than 10%, except for those near and below the ca. 1 μg limit of resolution of the balance.

[c] Th/U model ratio inferred from 208/206 ratio and age of sample.

[d] Pbc = total common Pb in sample (initial + blank).

[e] Raw data corrected for fractionation.

[f] Corrected for fractionation, spike, blank and initial common Pb; error calculated by propagating the main sources of uncertainty.

Table 2
Summary of U–Pb ages for sills and dykes.

Sample	Stratigraphy	Fig. 1 ref.	No. points	MSWD[a]	Age (Ma)	2 sigma
K08-31	Beaufort Gr.	12	3	2.5	182.7	0.9
QU1-2	Beaufort Gr.	13	2	1.4	182.7	0.3
K08-41	Beaufort Gr.	11	2 (of 3)	1.2	182.5	0.5
K08-1	Beaufort Gr.	6	3 (of 4)	1.5	183	0.5
K08-48	Beaufort Gr.	10	3 (of 4)	1.1	182.9	0.3
K08-47	Beaufort Gr.	9	3 (of 4)	1.6	182.4	0.7
SP08-05	Beaufort/Storm.	8	6	1.4	183	0.3
K08-6	Beaufort/Storm.	7	4	1	182.5	0.3
K08-9	Beaufort/Storm.	14	4 (of 5)	1.6	182.8	0.4
SP-07-05	Dyke	1	3	0.5	182.6	0.3
SP-06-05	Dyke	2	3	0.6	182.5	0.3
K08-34	Ecca Gr.	5	3	1.8	182.9	0.5
K08-13	Ecca Gr.	3	4 (of 5)	1.9	182.8	0.4
K08-16	Ecca Gr.	4	4	1.4	182.3	0.6
G39974-596 m[b]	Ecca Gr.	UZ1	5 (of 7)	1.9	182.5	0.4

[a] Conc + Equiv.
[b] From Svensen et al. (2007).

The interpretative sill architecture in Fig. 1 was digitized and imported into MATLAB to calculate the sill area in 2D. The results show that the sills comprise a total cross sectional area of 755 km^2, in which 350 km^2 is located in the Ecca Group. Since the Karoo Basin is elongated and the N/S Karoo Basin length is ~450 km, the total sill volume emplaced in the basin is 340,000 km^3 E (160,000 km^3 in the Ecca Group).

4.2. U–Pb results

We have extracted zircons from coarse-grained and pegmatitic samples of mafic sills and dykes across the basin (Fig. 1). Out of 23 processed samples, 14 gave zircon ($ZrSiO_4$; Fig. 2a–c) and/or baddeleyite (ZrO_2; Fig. 2d) that could be used for age determination. The resulting data are reported in Table 1 and the ages and regression parameters are summarized in Table 2. The quality of the analyzed zircons varied from very high (i.e., abundant prisms or fragments of clear non metamict zircon; Fig. 2a), to poor (i.e. few crystals, mostly with fractures, inclusions and altered domains; Fig. 2c). Despite the significant variations in terms of abundance and quality, all populations have similar basic characteristics with long-prismatic crystal shapes, widespread occurrence of broken and irregular fragments, dominance of {100} and {101} typologies, elevated Th/U ratios (1–4), and high to very high U contents (200–22,000 ppm) (Table 2).

The analyses in the different samples show a variation in the degree of precision, largely as a function of the quantity and quality of the material available. By focusing the analyses on the most pristine domains, i.e. those free of alteration, fractures and other imperfections. Even from small grains, it was possible to produce data with a minimum of Pb loss and there are few outliers. Only four of the

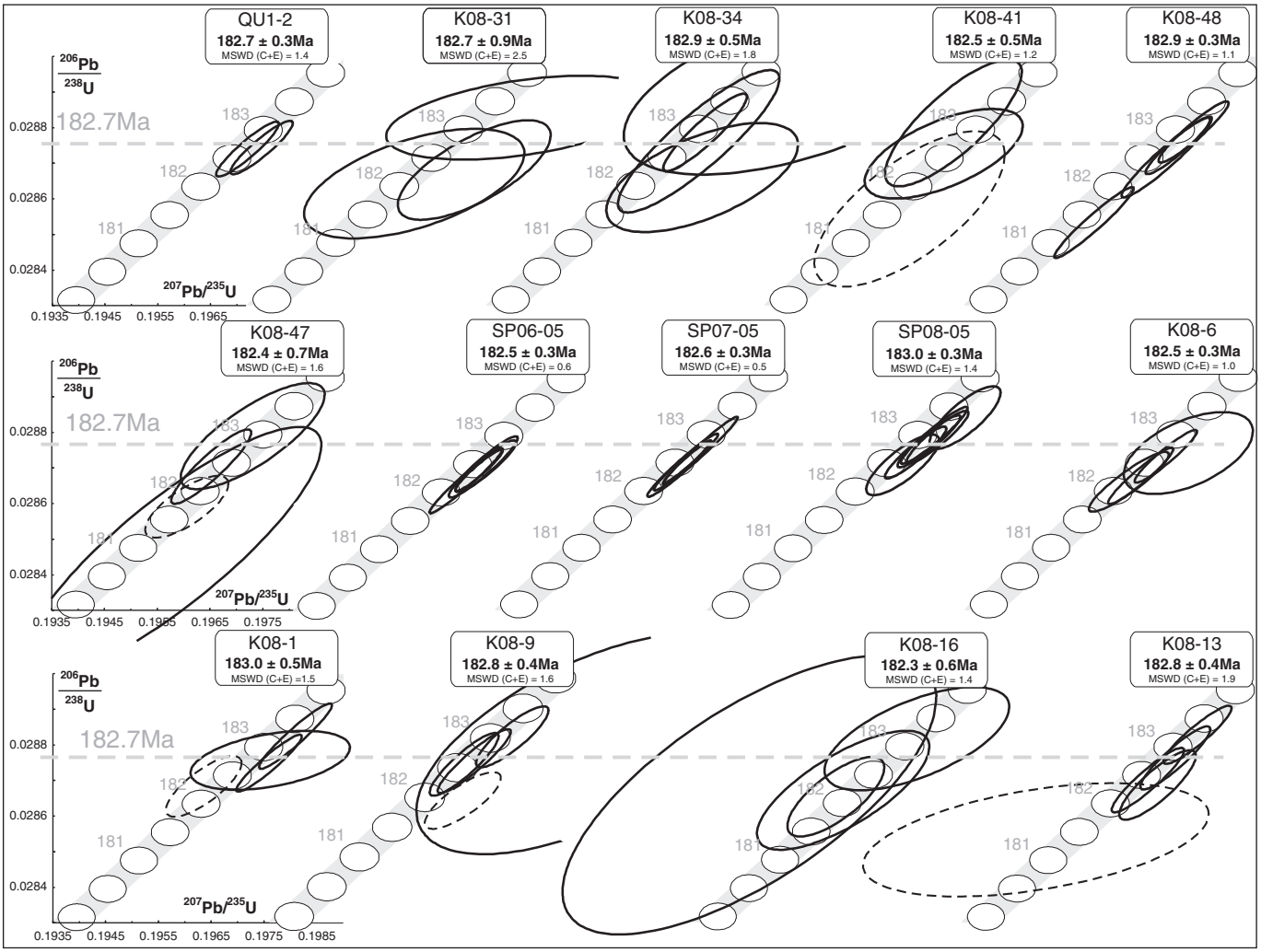

Fig. 3. Stacked concordia diagram for samples in this study (Table 1). The ellipses indicate the 2-sigma uncertainty. Stippled ellipses indicate results that were not considered in the age calculation due to their excessive discordance.

analyses had to be rejected because of Pb loss, revealed as slightly younger ages. Other analyses may also be affected by subordinate amounts of Pb loss but their discordance is no longer resolvable. Inherited cores were not a problem with these populations although few isolated subrounded zircon grains of probable xenocrystic origin were observed in some of the samples.

Chemical abrasion gave results that are consistent with the mechanically abraded ones when tested on non-metamict zircon (SP08-05). However, using chemical abrasion on metamict, fractured and altered zircons yielded data that are more discordant than those obtained by mechanical abrasion (Table 1, Fig. 3). This behavior reflects a fundamental difference between zircon in mafic and felsic rocks: the zoned nature and lower U content of the latter favor the chemical abrasion technique, which will separate concordant and discordant zircon domains. In contrast, the very high U content of mafic zircons (caused by the relatively high U/Zr ratios of residual melt of crystallizing bodies) creates a high degree of metamictization that cannot be annealed. In addition, the scarcity of low-U zones in mafic zircons limits the ability of the crystal to isolate annealed domains during partial dissolution in HF, thus dissolving most of the zircon with little left for analysis. Nevertheless, good results were obtained by chemical abrasion of zircon grains from sample SP08-05, which contained a large population of good quality zircons.

Baddeleyite is present in several of the samples, but generally as very thin blades with a high ratio of surface to volume, that are too thin to abrade and hence will likely have too low U–Pb ages due to the loss of Pb from the outer rims of the crystals. Only two samples, contained large and thick baddeleyite crystals which could be subjected to mechanical abrasion. These abraded grains are small, have lower U-contents (Table 1), and provide less precise, but concordant results overlapping those of the coexisting zircons.

The most precise data sets tend to lie to the right of the Concordia curve, a feature that at least in part can be explained by a presumable bias in the currently used set of decay constants (Mattinson, 2010; Schoene et al., 2006). The ages were therefore calculated by averaging the $^{206}Pb/^{238}U$ values. The results vary from 183.0 ± 0.5 to 182.3 ± 0.6 myr. There are only few hints of potential age variations, for example sample SP08-05 with an age of 183.0 ± 0.3 does not overlap very tightly with the two precise ages for the Gap Dyke samples of 182.5 and 182.6 ± 0.3 myr (SP06-05 and SP07-05). A slightly younger age of the Gap Dyke would be consistent with the field evidence of inclusions of dolerite in the dykes, but the resolution is not conclusive enough to allow such a distinction.

All samples yielded a coherent data set (Fig. 3, Table 2) irrespective of the geographic and stratigraphic position of the sample. The weighted mean age without taking the dating uncertainty into account is 182.7 ± 0.1 myr where the 2-sigma standard deviation gives an uncertainty interval of 200 ka and assuming that all the sills represent one event with zero duration.

4.3. Monte Carlo simulations

The resulting cumulative probability distribution (of deviation in the given dates as large as observed) as a function of standard deviation (1-sigma duration) of the emplacement events is shown in Fig. 4b. The statistical modeling gives a probability of 95% that the true standard deviation of the emplacement events was less than 0.23 myr. (corresponding to a 2-sigma of ± 0.46 myr.). Such a standard deviation translates into a total duration of less than 0.90 myr. for 95% of the emplacement events. A 95% probability bound on the smallest possible duration could not be assigned, as more than 50% of the standard deviations from the simulations exceeded the observed deviation even for $\sigma_{sim} = 0$ myr. (Fig. 4b). This means that an instantaneous emplacement of all analyzed sills cannot be rejected. However, the most likely standard deviation of emplacement events is given by the highest slope of the cumulative probability distribution

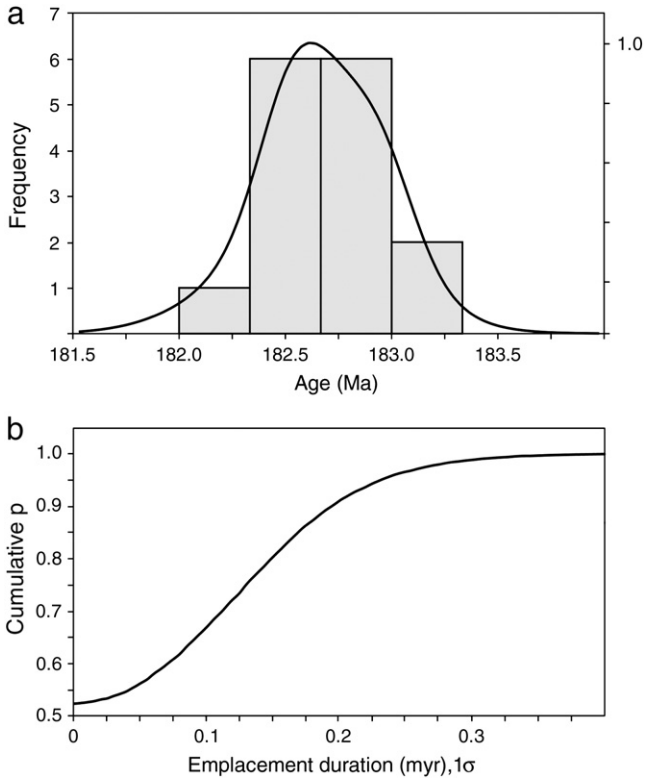

Fig. 4. Statistical analysis. (a) Histogram of U–Pb radiometric dates, and a smooth density estimate based on the given errors. (b) Cumulative probability distribution of 1-sigma width of the assumed Gaussian intensity of emplacement through time (myr).

in Fig. 4b, which is equivalent to 0.12 myr. This suggests that 95% of the sills were emplaced within 0.47 myr.

This result can be compared with simple error propagation of the difference between the oldest date of 183.0 ± 0.25 myr (2-sigma) and the youngest date of 182.3 ± 0.30 myr, giving a total duration of 0.7 ± 0.20 myr. (1-sigma). This translates into a 95% probability that the total duration was less than 1.0 myr. Instantaneous emplacement (duration 0 myr.) can seemingly be rejected at $p<0.05$ with this method. This can be explained by the fact that selecting the oldest and youngest dates produces a statistical bias towards longer duration. The Monte Carlo method avoids this bias by taking all dates into account.

4.4. Melt emplacement rates

The volume of sills in the Karoo Basin, estimated from regional cross sections calibrated by borehole information, is about 340,000 km^3. This corresponds to 367,000 km^3 of magma when corrected for the 8% volume reduction from melt to solid. Combining these volumes with the most likely maximum duration of emplacement (0.47 myr), the minimum magma flux is accordingly 0.78 km^3/yr.

5. Discussion

5.1. Basin-scale emplacement

The previously suggested prolonged sill emplacement and late stage volcanism at about 178 myr (Jourdan et al., 2008) is not supported by the new U–Pb zircon data. Even though the sill giving the $^{40}Ar/^{39}Ar$ age of 176.2 ± 1.3 myr (Jourdan et al., 2008) was not redated in our study, there are no indications of volcanism younger than 181.8 myr even when considering the full range of the 2-sigma uncertainties (Fig. 4a). The general absence of crosscutting

relationships between sills in the field suggests furthermore that the sills were emplaced as a coherent complex in a short period of time. The few sills showing evidence for multiple magma injections (Galerne et al., 2008) unfortunately yielded no zircons. It is however remarkable that a sill contaminated by sedimentary rocks (K08-48), which also cuts an extensive dolerite sill, does not have a younger age compared to the rest of the samples. Crystallization of a 100 m thick sill intrusion takes place on a timescale of 1000 yrs, which can explain why the major Gap Dyke (SP-06-05 and SP-07-05) gave similar results to the sills even though the dyke contains xenoliths of sill material.

5.2. Emplacement rates

The combined age modeling and sill volume estimates give an average melt emplacement rate of 0.78 km^3/yr (367,000 km^3 melt, 0.47 myr.). This suggests that the magma flux into the Karoo Basin was much higher than the 0.3 km^3/yr previously estimated for the rate of melt extraction from the mantle over the ~6 myr. volcanism in Southern Africa (Jourdan et al., 2005). High emplacement rates of melt into the Karoo Basin are also supported by another line of arguments. The volumes of individual sills in the Karoo Basin may exceed 3000 km^3, which results in fluxes of 60–300 km^3/yr when averaged over 10–50 yrs emplacement times. These extreme rates are comparable to those for super-eruptions with the eruption of >400 km^3 of magma in months to years (Bryan et al., 2010), and the rapid emplacement of individual Columbia River LIP lava flows (~125 km^3/yr, 6–14 yr duration) (Self et al., 1997) and Deccan Traps lava flows (30–300 km^3/yr, (Chenet et al., 2009)). In general, magma storage in the upper crust may explain high emplacement rates (Bryan et al., 2010), for which ascent of magma from the upper mantle is not a rate limiting step. This was recently supported by new geochemical data from the Karoo Basin sills suggesting shallow fractional crystallization (Neumann et al., 2011). Thus the most likely emplacement model includes intervals with very high rates and a short total period of emplacement across the basin.

5.3. The Karoo LIP and the Toarcian event

The sills we dated have ages overlapping the ages of the initiation of the Toarcian Oceanic Anoxic Event (182.16 ± 0.6 myr) (Mazzini et al., 2010), and the rapid emplacement of magma into the Karoo Basin strengthens the hypothesis about a causal link between the resulting contact metamorphism and the Toarcian carbon cycle perturbation (Svensen et al., 2007). Both the steady-state emplacement of magma and the pulsed emplacement of a few major magma batches over a 0.47 myr. period are in agreement with Toarcian proxy data (Cohen et al., 2007). By analogy with the end-Permian crisis and sill emplacement in the Tunguska Basin, East Siberia, even individual large-scale sills may give rise to substantial modifications of the global climate (Roscher et al., 2011).

6. Conclusions

Basaltic sill intrusions and dikes in the Karoo Basin have yielded zircons suitable for high-quality U–Pb dating. We show that:

- Sills across the Karoo Basin have overlapping ages within small errors ranging from 183.0 ± 0.5 to 182.3 ± 0.6 myr.
- Monte Carlo simulations demonstrate that emplacement could have taken place in less than 0.47 myr., and may even represent a single emplacement event.
- We estimate the volume of melt emplaced in the basin to 367,000 km^3, which results in an average melt emplacement rate of 0.78 km^3/yr. Even though individual sills may represent emplacement rates of >60 km^3/yr, our results are higher than previous estimates for the Karoo LIP.

Acknowledgments

We gratefully acknowledge support from the Norwegian Research Council (a PetroMaks grant and a YFF grant to H. Svensen, and a Centre of Excellence grant to PGP), Mr. Goddard for assistance in the field, and Rhodes University for providing field equipment. We would like to express our gratitude for being allowed entry to quarries across South Africa and for access to the core library of the Council for Geoscience in Pretoria (handled by David Motloi).

Appendix A. Supplementary data

Supplementary data to this article can be found online at doi:10.1016/j.epsl.2012.01.015.

References

Bryan, S.E., Peate, I.U., Peate, D.W., Self, S., Jerram, D.A., Mawby, M.R., Marsh, J.S., Miller, J.A., 2010. The largest volcanic eruptions on Earth. Earth Sci. Rev. 102, 207–229.
Catuneanu, O., Wopfner, H., Eriksson, P.G., Cairncross, B., Rubidge, B.S., Smith, R.M.H., Hancox, P.J., 2005. The Karoo basins of south-central Africa. J. Afr. Earth Sci. 43, 211–253.
Chenet, A.-L., Courtillot, V., Fluteau, F., Gérard, M., Quidelleur, X., Khadri, S.F.R., Subbarao, K.V., Thordarson, T., 2009. Determination of rapid Deccan eruptions across the Cretaceous–Tertiary boundary using paleomagnetic secular variation: 2. Constraints from analysis of eight new sections and synthesis for a 3500-m-thick composite section. J. Geophys. Res. 114, B06103.
Chevallier, L., Woodford, A., 1999. Morpho-tectonics and mechanism of emplacement of the dolerite rings and sills of the western Karoo, South Africa. S. Afr. J. Geol. 102, 43–54.
Cohen, A.S., Coe, A.L., Kemp, D.B., 2007. The late Palaeocene–Early Eocene and Toarcian (Early Jurassic) carbon isotope excursions: a comparison of their time scales, associated environmental changes, causes and consequences. J. Geol. Soc. 164, 1093–1108.
Corfu, F., 2004. U–Pb age, setting and tectonic significance of the anorthosite–mangerite–charnockite–granite suite, Lofoten-Vesteralen, Norway. J. Petrol. 45, 1799–1819.
du Toit, A.I., 1920. The Karoo dolerites of South Africa: a study in hypabyssal injection. Trans. Geol Soc. S. Af. 23, 1–42.
Duncan, R.A., Hooper, P.R., Rehacek, J., Marsh, J.S., Duncan, A.R., 1997. The timing and duration of the Karoo igneous event, southern Gondwana. J. Geophys. Res. 102, 18127–18138.
Eales, H.V., Robey, J.A., 1976. Differentiation of tholeiitic Karroo magma at Birds River, South Africa. Contrib. Mineral. Petrol. 56, 101–117.
Encarnacion, J., Fleming, T.H., Elliot, D.H., Eales, H.V., 1996. Synchronous emplacement of Ferrar and Karoo dolerites and the early breakup of Gondwana. Geology 24, 535–538.
Galerne, C.Y., Neumann, E.R., Planke, S., 2008. Emplacement mechanisms of sill complexes: information from the geochemical architecture of the Golden Valley Sill Complex. S. Afr. J. Volcanol. Geoth. Res. 177, 425–440.
Jaffey, A.H., Flynn, K.F., Glendenin, L.E., Bentley, W.C., Essling, A.M., 1971. Precision measurements of half-lives and specific activities of ^{235}U and ^{238}U. Phys. Rev. C 4, 1889–1906.
Johnson, M.R., Van Vuuren, C.J., Hegenberger, W.F., Key, R., Shoko, U., 1996. Stratigraphy of the Karoo Basin in Southern Africa: an overview. J. Afr. Earth Sci. 23, 3–15.
Jourdan, F., Féraud, G., Bertrand, H., Kampunzu, A.B., Tshoso, G., Watkeys, M.K., Le Gall, B., 2005. Karoo large igneous province: brevity, origin, and relation to mass extinction questioned by new $^{40}Ar/^{39}Ar$ age data. Geology 33, 745–748.
Jourdan, F., Féraud, G., Bertrand, H., Watkeys, M.K., Renne, P.R., 2007. Distinct brief major events in the Karoo large igneous province clarified by new $^{40}Ar/^{39}Ar$ ages on the Lesotho basalts. Lithos 98, 195–209.
Jourdan, F., Féraud, G., Bertrand, H., Watkeys, M.K., Renne, P.R., 2008. The $^{40}Ar/^{39}Ar$ ages of the sill complex of the Karoo large igneous province: implications for the Pliensbachian–Toarcian climate change. Geochem. Geophys. Geosyst. 9, Q06009.
Krogh, T.E., 1973. Low-contamination method for hydrothermal decomposition of zircon and extraction of U and Pb for isotopic age determinations. Geochim. Cosmochim. Acta 37, 485–494.
Krogh, T.E., 1982. Improved accuracy of U Pb zircon ages by the creation of more concordant systems using an air abrasion technique. Geochim. Cosmochim. Acta 46, 637–649.
Ludwig, K.R., 2003. Isoplot 3.0. A Geochronological Toolkit for Microsoft Excel. Berkeley Geochron. Center. Spec. Publ. No. 4.
Marsh, J.S., Eales, H.V., 1984. The chemistry and petrogenesis of igneous rocks of the Karoo central area, Southern Africa. Spec. Publ. Geol. Soc. S. Afr. 13, 27–67.
Mattinson, J.M., 2005. Zircon U–Pb chemical abrasion ("CA-TIMS") method: combined annealing and multi-step partial dissolution analysis for improved precision and accuracy of zircon ages. Chem. Geol. 220, 47–66.

Mattinson, J.M., 2010. Analysis of the relative decay constants of ^{235}U and ^{238}U by multi-step CA-TIMS measurements of closed-system natural zircon samples. Chem. Geol. 275, 186–198.

Mazzini, A., Svensen, H., Leanza, H.A., Corfu, F., Planke, S., 2010. Early Jurassic shale chemostratigraphy and U–Pb ages from the Neuquén Basin (Argentina): implications for the Toarcian Oceanic Anoxic Event. Earth Planet. Sci. Lett. 297, 633–645.

McClintock, M., White, J.D.L., Houghton, B.F., Skilling, I.P., 2008. Physical volcanology of a large crater-complex formed during the initial stages of Karoo flood basalt volcanism, Sterkspruit, Eastern Cape, South Africa. J. Volcanol. Geotherm. Res. 172, 93–111.

Moulin, M., Fluteau, F., Courtillot, V., Marsh, J., Delpech, G., Quidelleur, X., Gérard, M., Jay, A.E., 2011. An attempt to constrain the age, duration, and eruptive history of the Karoo flood basalt: Naude's Nek section (South Africa). J. Geophys. Res. 116, B07403.

Neumann, E.-R., Svensen, H., Galerne, C.Y., Planke, S., 2011. Multistage Evolution of Dolerites in the Karoo Large Igneous Province, Central South Africa. J. Petrol. 52, 959–984.

Roscher, M., Stordal, F., Svensen, H., 2011. The effect of global warming and global cooling on the distribution of the latest Permian climate zones. Palaeogeogr. Palaeoclimatol. Palaeoecol. 309, 186–200.

Schoene, B., Crowley, J.L., Condon, D.J., Schmitz, M.D., Bowring, S.A., 2006. Reassessing the uranium decay constants for geochronology using ID-TIMS U–Pb data. Geochim. Cosmochim. Acta 70, 426–445.

Self, S., Thordarson, T., Keszthelyi, L., 1997. Emplacement of continental flood basalt lava flows. In: Mahoney, J.J., Coffin, M.F. (Eds.), Large Igneous Provinces: Continental, Oceanic, and Planetary Flood Volcanism: AGU - Geophys. Monogr., 100, pp. 381–410.

Smith, R.M.H., 1990. A review of stratigraphy and sedimentary environments of the Karoo basin of South Africa. J. Afr. Earth Sci. 10, 117–137.

Svensen, H., Jamtveit, B., Planke, S., Chevallier, L., 2006. Structure and evolution of hydrothermal vent complexes in the Karoo Basin, South Africa. J. Geol. Soc. 163, 671–682.

Svensen, H., Planke, S., Chevallier, L., Malthe-Sorenssen, A., Corfu, F., Jamtveit, B., 2007. Hydrothermal venting of greenhouse gases triggering Early Jurassic global warming. Earth Planet. Sci. Lett. 256, 554–566.